Industrial Chemistry & Materials

ROYAL SOCIETY OF CHEMISTRY

PAPER

View Article Online
View Journal | View Issue

Cite this: *Ind. Chem. Mater.*, 2024, **2**, 600

Cross-polymerization between bio-oil and polyaniline: synergistic effects on pore development in subsequent activation and adsorption of phenol†

Baihong Li,[a] Chao Li,[a] Dianqiang Li,[a] Lijun Zhang,[a] Shu Zhang,[b] Yi Wang,[c] Song Hu,[c] Jun Xiang,[c] Mortaza Gholizadeh[d] and Xun Hu *[a]

Bio-oil is a major product from pyrolysis of biomass which serves as a carbon source to produce carbon material due to its high reactivity towards polymerization itself or cross-polymerization with other organic feedstocks. In this study, activation of polyaniline (PANI) mixed with wheat straw-derived bio-oil and $K_2C_2O_4$ at 800 °C was conducted, aiming to understand the effect of potential interactions of bio-oil with PANI on pore development of resulting activated carbon (AC). The results revealed cross-polymerization reactions between PANI and bio-oil during direct activation, which increased the yield of AC from 13.0% (calculated average) to 15.0%, the specific surface area from 1677.9 m^2 g^{-1} (calculated average) to 1771.3 m^2 g^{-1}, and the percentage of micropores from 94.3% to 97.1%. In addition, pre-polymerization of PANI and bio-oil at 200 °C before activation was also conducted. Such pretreatment could increase the AC yield from 13.0% to 23.3%, but the specific surface area decreased to 1381.8 m^2 g^{-1}. The pre-polymerization formed the organics that were more resistant towards cracking/gasification, but introduced oxygen-rich functionalities. This made AC highly hydrophilic, rendering a much higher capability for adsorption of phenol despite the smaller specific surface area. Additionally, the AC with developed pore structures facilitated dispersion of nickel in Ni/AC and enhanced the catalytic activity for hydrogenation of *o*-chloronitrobenzene and vanillin.

Received 6th January 2024,
Accepted 7th February 2024

DOI: 10.1039/d4im00001c

rsc.li/icm

Keywords: Polyaniline; Bio-oil; Activation; Activated carbon; Pre-polymerization; Adsorption.

1 Introduction

Pyrolysis is an important thermochemical route to convert bulky biomass to biochar and bio-oil of much higher volumetric energy density as well as pyrolytic gases that can be combusted *in situ*.[1–3] Biochar has versatile applications, while bio-oil is commonly accepted as an intermediate product for production of biofuel *via* further hydrotreatment.[4–6] However, owing to the high oxygen content, high acidity and high reactivity of the organics in bio-oil towards polymerization, hydrotreatment of bio-oil for deoxygenation is rather challenging due to rapid coking and deactivation of the catalyst, making the process costly.[7–10]

The high tendency of organics in bio-oil to polymerize is an issue for hydrotreatment, which, however, is highly desirable in the preparation of carbonaceous materials. Moreover, Fan *et al.* indicated that bio-oil is nearly ash-free[11] and bio-oil-based materials avoid the inheritance or interference of biological structures of biomass. This makes bio-oil a suitable precursor for the preparation of carbon materials. Nonetheless, bio-oil is composed of condensable volatiles, implying high volatility of organics in bio-oil during heating, which diminishes the yield of solid carbonaceous material.[12,13] For example, the study by Li *et al.* showed that the yield of coke derived from heating of heavy components in bio-oil was only 2.73% without adding template material or additives.[14] To tackle this issue, Hu *et al.* proposed cross-polymerization of bio-oil with furfural, which remarkably enhanced the yield of carbonaceous material.[15] Furfural can be produced from biomass *via* hydrolysis or pyrolysis,[16–18] and opening of its furan ring during hydrolysis generates reactive intermediates,[19–21] facilitating polymerization of the organics

[a] *School of Material Science and Engineering, University of Jinan, Jinan, 250022, P. R. China. E-mail: Xun.Hu@outlook.com*
[b] *College of Materials Science and Engineering, Nanjing Forestry University, Nanjing, 210037, P. R. China*
[c] *State Key Laboratory of Coal Combustion, Huazhong University of Science and Technology, P. R. China*
[d] *Pyrochar Company, Notting Hill, Victoria 3168, Australia*
† Electronic supplementary information (ESI) available. See DOI: https://doi.org/10.1039/d4im00001c

in bio-oil. Nonetheless, furfural will not work in the preparation of heteroatoms such as N-doped carbon material from bio-oil. Externally added nitrogen-containing organics are required to cross-react with the organics in bio-oil.

Herein, polyaniline (PANI) was used for the preparation of N-doped porous carbon material from bio-oil. PANI was selected as a nitrogen source, which was based on the consideration that it is alkaline and contains a benzene ring for the occurrence of polymerization *via* electrophilic substitution reactions. The generated product will unavoidably be impacted by a cross-reaction between PANI and bio-oil. Thus, PANI and bio-oil were mixed in various ratios and pre-polymerized at 200 °C to form a carbonaceous material, which was then activated with $K_2C_2O_4$ at 800 °C to prepare activated carbon (AC). Direct activation of the mixture of PANI and bio-oil was also conducted for comparison. The obtained AC was used for adsorption of phenol from the aqueous phase and also as a carrier of nickel catalyst for hydrogenation of *o*-chloronitrobenzene and vanillin. The research scheme is shown in Scheme 1. Additionally, the development of functional groups of AC from activation of the carbonaceous material from the polymerization of PANI and bio-oil was investigated with *in situ* diffuse reflectance infrared Fourier transform spectroscopy (DRIFTS). The results indicated that cross-polymerization between PANI and bio-oil existed and was a determining factor for development of the pore structures, functionalities, and capabilities of the resulting ACs for adsorption of phenol from the aqueous phase.

2 Results and discussion

2.1 Yields of the pyrolysis and activation products

The distribution of products from the pyrolysis or activation of PANI, bio-oil or their mixture at 800 °C is shown in Fig. 1 and S2.† For the pyrolysis of PANI, bio-oil or their mixture (P1B1), the yield of bio-oil was higher (39.1% *vs.* 33.9% average value) with the mixture as a feedstock. This was at the cost of biochar (35.3% *vs.* 38.9% from average value). The heavy organics in bio-oil could react with PANI, but the thermally unstable nature of the organics led to the formation of condensable volatiles but not solid residue. PANI also interfered with aromatization of heavy phenolics during the pyrolysis. Pyrolysis of PANI generated more gases than bio-oil, while the activation of PANI with $K_2C_2O_4$ further significantly increased the formation of bio-oil *via* cracking routes, producing AC with a very low yield (10.0%).

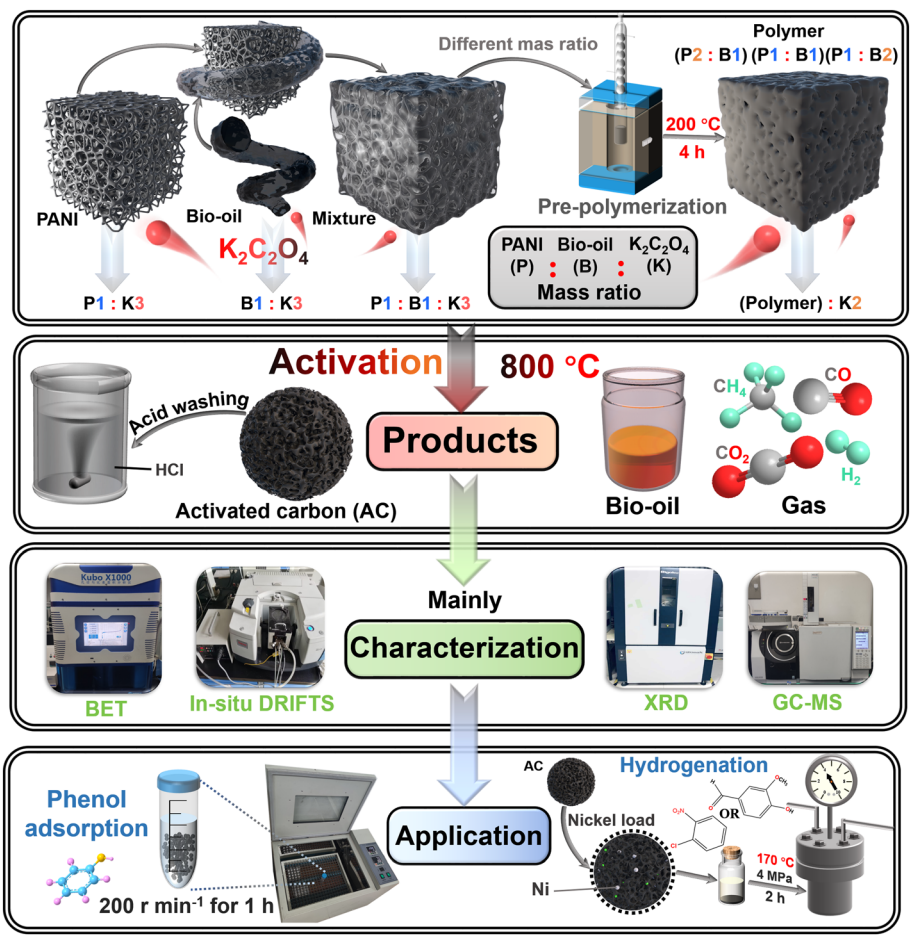

Scheme 1 The research scheme for the direct activation or pre-polymerization plus activation of polyaniline and bio-oil.

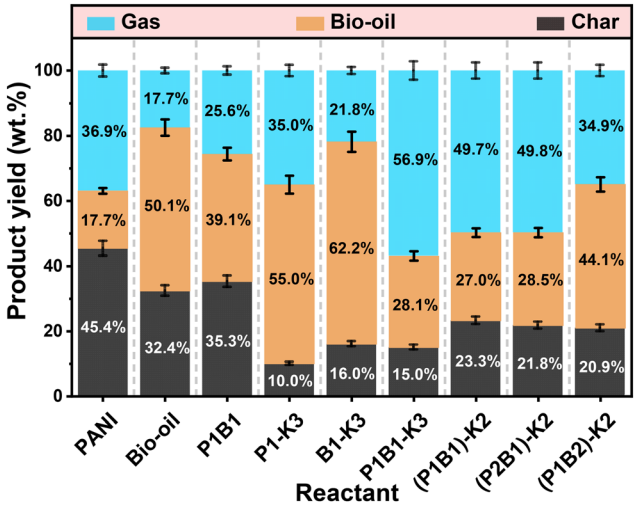

Fig. 1 The yields of gas, biochar/activated carbon and bio-oil from the pyrolysis or activation of polyaniline, bio-oil or their mixture of different mass ratios at 800 °C. P1B1: PANI and bio-oil mixed at a mass ratio of 1 : 1; P1-K3: PANI and $K_2C_2O_4$ mixed at a mass ratio of 1 : 3; B1-K3: bio-oil and $K_2C_2O_4$ mixed at a mass ratio of 1 : 3; P1B1-K3: PANI, bio-oil and $K_2C_2O_4$ mixed at a mass ratio of 1 : 1 : 3; (P1B1)-K2: PANI and bio-oil pre-polymerized at a ratio of 1 : 1 and then mixed with $K_2C_2O_4$ at a ratio of 1 : 2; (P2B1)-K2: PANI and bio-oil pre-polymerized at a ratio of 2 : 1 and then mixed with $K_2C_2O_4$ at a ratio of 1 : 2; (P1B2)-K2: polyaniline and bio-oil pre-polymerized at a ratio of 1 : 2 and then mixed with $K_2C_2O_4$ at a ratio of 1 : 2.

Activation of bio-oil with $K_2C_2O_4$ also formed gases as the main product, while the heavy organics in the bio-oil were more resistant to the cracking/gasification reactions induced by the high temperature and $K_2C_2O_4$, generating AC of a higher yield (16.0%). Moreover, activation of the mixture of PANI and bio-oil (P1B1-K3) formed a relatively higher yield of AC (15.0% *vs.* 13.0% from average value), attributed to the occurrence of cross-polymerization between PANI and organics in bio-oil during the activation. Similarly, the pre-polymerization of PANI and bio-oil at 200 °C for 4 h could also enhance the thermal stability of the organics and their resistivity towards cracking/gasification, especially for the ones with a mass ratio of 1 : 1 for PANI and bio-oil. The detailed composition of the bio-oil formed was further analyzed.

2.2 Characterizations of bio-oil

The relative abundance of light organics generated during the pyrolysis and activation of the bio-oil and PANI mixture is shown in Fig. 2a and Table S1.† The components in the liquid products from the pyrolysis of PANI and bio-oil were relatively simple, including mainly phenols (*i.e.* phenol, 4-ethyl-2-methoxy-phenol and 2-methoxy-4-methyl-phenol) and benzenes (*i.e.* styrene), nitrogen-containing organics (*i.e.* aniline and diphenylamine) and a small portion of ketones (*i.e.* 4-cyclopentene-1,3-dione and 3-methyl-1,2-cyclopentanedione). This was due to the degradation of PANI and the further cracking of heavy pyrolytic lignin and sugar oligomers in the heavy bio-oil. The activation with $K_2C_2O_4$ further reduced the abundance of these light components in the liquid products. The presence of $K_2C_2O_4$ led to essential cracking of these organic compounds into gases (Fig. 1). For example, the abundance of phenolics like phenol and 4-ethyl-2-methoxy-phenol, the nitrogen-containing organics like aniline and 2-hydroxy-benzonitrile, and even the benzenes like styrene decreased remarkably in the activation (Table S1†). The promotional effect of $K_2C_2O_4$ on cracking/gasification also impacted the evolution of the heavy organics.

Fig. 2b–d show UV fluorescence spectra of the heavy organics in the liquid products. Three main peaks located at 296, 324 and 343 nm in the 2D UV fluorescence spectra (Fig. 2b) are attributed to the organics with equivalent single to multi-benzene ring structures.[22] The activation with $K_2C_2O_4$ significantly reduced the abundance of the fluorescence peaks, especially the one at 343 nm, reflecting the high activity of $K_2C_2O_4$ for cracking. Similar conclusions could be extracted in the 3D fluorescence spectra in Fig. 2c and d. Regions IV and V represent heavy organics with tryptophan-like and humic acid-like structures, respectively.[23] $K_2C_2O_4$ led to significant cracking of the humic acid-like organics, while the abundance of tryptophan-like organics also decreased remarkably.

2.3 Biochar and AC characterization

2.3.1 BET analysis. Table 1 shows the pore structures of the AC and biochar generated by activation or pyrolysis of PANI and/or bio-oil. The pore development of the biochar from the pyrolysis of PANI and bio-oil at 800 °C (Biochar-P1B1) was rather limited (79.1 $m^2\ g^{-1}$). Through the activation with $K_2C_2O_4$, the pore structures of the AC from PANI only (AC-P1-K3) developed remarkably, reaching a specific surface area of 2060.6 $m^2\ g^{-1}$. Sufficient cracking of PANI in the presence of $K_2C_2O_4$ formed the developed pore structures. In contrast, the AC from activation of the bio-oil (AC-B1-K3) showed a lower specific surface area (1295.1 $m^2\ g^{-1}$), but also with a lower proportion of micropores (93.3% *versus* 95.2% from PANI). The organics in the bio-oil were less prone to be cracked than that from PANI. Although the activation of the mixture of PANI and bio-oil (AC-P1B1-K3) did not produce AC of higher specific surface area than that of AC-P1-K3 (1771.3 $m^2\ g^{-1}$ *vs.* 2060.6 $m^2\ g^{-1}$), the number exceeded the calculated average (1677.9 $m^2\ g^{-1}$) of that of AC-P1-K3 and AC-B1-K3. This suggested the synergistic effect between PANI and bio-oil for creating more porous structures, originating from their cross-polymerization reactions.

The pre-polymerization PANI and bio-oil at 200 °C also affected the evolution of the pore structure of ACs. AC-(P2B1)-K2 with higher abundance of PANI still possessed a higher specific surface area (1676.1 $m^2\ g^{-1}$) than the counterparts. AC-(P1B1)-K2 showed a higher mass yield (Fig. 1), which was achieved at the expense of the specific surface area (1381.8 $m^2\ g^{-1}$). Additionally, the activation of the samples with the coexistence of PANI and bio-oil all showed a higher proportion of micropores (≥96.6%) than that from only PANI

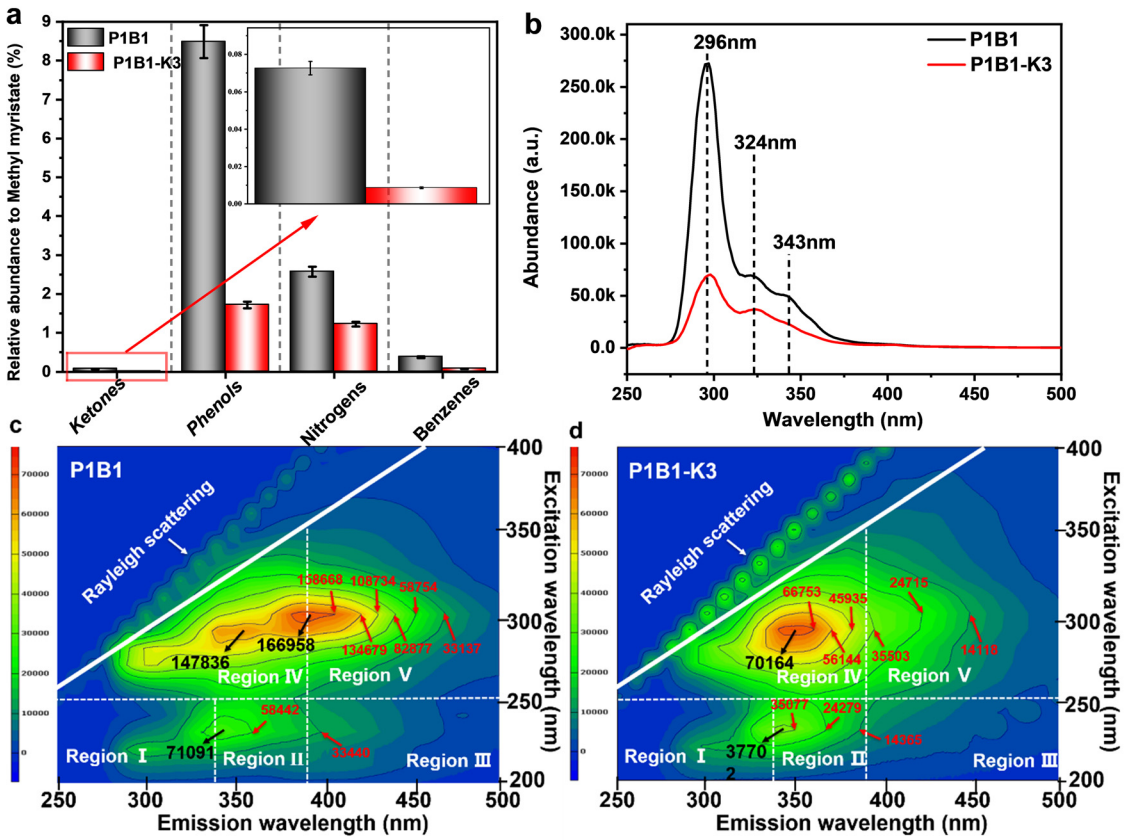

Fig. 2 GC-MS and UV-fluorescence spectra of the bio-oil produced from the pyrolysis or activation of the mixture of polyaniline and bio-oil with a mass ratio of 1 : 1 at 800 °C. (a) Normalized abundance of the typical compounds found in the bio-oils; (b) 2D UV-fluorescence spectra of the bio-oils; (c and d) 3D UV-fluorescence spectra of the bio-oils.

Table 1 Pore analysis of the biochar and activated carbon produced from the activation of polyaniline, bio-oil or their mixture of different mass ratios at 800 °C

Entry	Samples	S_{BET}[a] ($m^2\ g^{-1}$)	V_b[b] ($cm^3\ g^{-1}$)	S_{micro}[c] ($m^2\ g^{-1}$)	V_{micro}[d] ($cm^3\ g^{-1}$)	D_a[e] (nm)
1	Biochar-P1B1	79.1	0.63	79.1(100%)	0.0055(0.8%)	31.9
2	AC-P1-K3	2060.6	1.8	1962.1(95.2%)	1.4(81.6%)	3.4
3	AC-B1-K3	1295.1	0.79	1208.0(93.3%)	0.47(60.0%)	2.4
4	AC-P1B1-K3	1771.3	1.2	1720.3(97.1%)	0.86(79.4%)	2.7
5	AC- (P1B1)-K2	1381.8	0.73	1340.1(97.0%)	0.58(78.9%)	2.1
6	AC- (P2B1)-K2	1676.1	1.0	1619.2(96.6%)	0.77(73.3%)	2.5
7	AC- (P1B2)-K2	1411.9	0.83	1372.1(97.2%)	0.56(67.8%)	2.3

[a] S_{BET} is the specific surface area obtained by the BET method. [b] V_b is the total pore volume at $P/P_0 = 0.99$. [c] S_{micro} is the micropore surface area; the percentage of S_{micro}/S_{BET} is given in parentheses. [d] V_{micro} is the micropore volume; the percentage of V_{micro}/V_t is indicated in parentheses. [e] D_a is the average pore diameter.

(≥95.2%) or only bio-oil (≥93.3%). The formation of polymeric products from the cross-polymerization facilitated the formation of micropores. The adsorption–desorption curves of the ACs in Fig. 3 showed a rapid increase in adsorption volume when P/P_0 was below 0.01. Moreover, when P/P_0 was higher than 0.2, the curve approached a horizontal plateau, which conformed to a Type I curve, indicating that the pores in AC were mainly micropores with a small amount of mesopores.[23,24] $K_2C_2O_4$ could promote the development of the mesoporous structure of AC from PANI, forming mesopores of larger size (Fig. 3b). In contrast, for the formation of micropores, the activation of bio-oil or the mixture of PANI and bio-oil with a higher bio-oil content formed micropores of larger pore sizes.

2.3.2 Elemental analysis. The content of the elements in AC is shown in Fig. 3c and d. Although all the ACs were washed with acid *via* the same procedure, there was still some residual ash retained in the AC due to the mutual coverage between inorganics. PANI is rich in N and some N-containing species were retained in the resulting AC. The

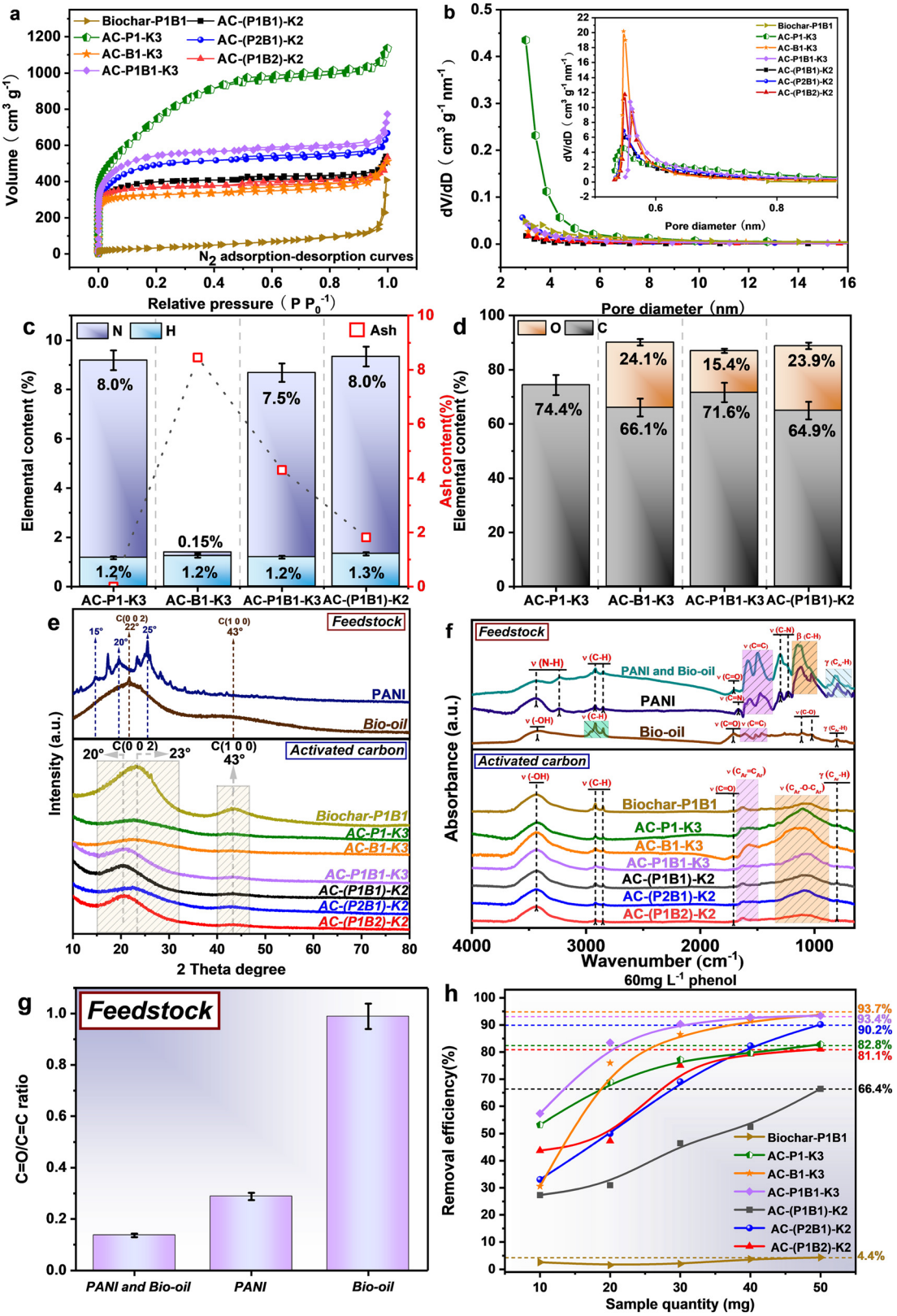

Fig. 3 Characterization of activated carbon. (a and b) Pore characteristics of the activated carbon; (c and d) elemental analysis of activated carbon (O = 100% − C% − H% − N% − S% − H_2O% − ash%); (e) XRD characterization; (f) FT-IR characterization; (g) the C═O/C═C ratio of feedstocks in FT-IR characterization; (h) the removal efficiency of phenol by ACs.

oxygen content in AC-B1-K3 was 24.1%, while that from AC-P1B1-K3 was 15.4% higher than the average value (12.1%), suggesting that the cross-interactions during the activation of the mixture retained more oxygen. This was further verified in the AC-(P1B1)-K2 sample, as evidenced by the further increase of the oxygen content to 23.9%. The pre-condensation pretreatment helped to retain more oxygen-containing functionalities in the resulting AC. This together with the nitrogen-containing species was desirable for providing more adsorption sites and for reducing the hydrophilicity of the resulting AC, which will be discussed later.

2.3.3 XRD analysis. Fig. 3e shows the results of the XRD characterization of the biochar and ACs. The PANI feedstock exhibited several periodic peaks at 15°, 20° and 25°, which was attributed to its orientation ordering and unique structural units.[25,26] The biochar-P1B1 sample exhibited two high-intensity crystal carbon peaks at around 23° and 43° attributed to C (0 0 2)[27] and C (1 0 0), which were generated as a result of aromatization.[28] After activation of PANI with $K_2C_2O_4$, the C (0 0 2) peak shifted towards a lower angle (from 23° to 20°) and the peak intensity decreased significantly. The cracking reactions during the activation disrupted the crystal structure of AC, leading to an increase in the spacing between the (0 0 2) planes (from 0.3961 to 0.4348 nm), which caused lattice distortion. However, the peak positions of C (0 0 2) for the AC from the activation of PANI or bio-oil did not change, but the peak intensity was very low. The cross-polymerization between PANI and bio-oil enhanced the crystallinity of the AC owing to the formation of some thermally stable structures. This was especially evident for the AC-P1B1-K3, AC-(P1B1)-K2 and AC-(P1B2)-K2 samples with a higher proportion of bio-oil. These structures were more resistant towards cracking reactions during the activation, leading to higher yields of AC (Fig. 1) but lower development of pore structures of AC (Table 1).

The microcrystalline structure of ACs was further analyzed (Table S2†). The higher the stacking height (L_c) and the narrower the full-width at half-maximum (FWHM), the higher the degree of graphitization and the more orderly the arrangement of microcrystalline structure of AC. Compared with AC-P1-K3 and AC-B1-K3, the ACs obtained from the activation of mixtures of PANI and bio-oil exhibited lower FWHM and higher L_c. This once again proved that the cross-polymerization between PANI and bio-oil could form stable structures, which improved the carbonization degree of AC and promoted the orderliness of its microcrystalline structure.

2.3.4 FT-IR and hydrophilicity analysis. Fig. 3f shows the characterization results of FT-IR about the distribution of functional groups of the samples. The bio-oil contained a rich variety of organics, especially the oxygen-containing functional groups like –OH,[29] C═O and C–O with the absorption at 3424, 1708 and 1024–1111 cm^{-1}, respectively. The high ratio of C═O to C═C in the bio-oil further confirmed the higher abundance of C═O (Fig. 3g). PANI, on the other hand, is a polymer with nitrogen-containing functional groups such as N–H,[30] C═N and C–N located at 3436–3236, 1668 and 1226–1300 cm^{-1}, respectively.[31,32] After their mixing and reactions, the functionalities on the outside of the mixture were mainly governed by PANI. The ratio of C═O to C═C further decreased (Fig. 3g) due to the abundant benzene ring structures in PANI. Importantly, the abundance of C═N diminished, suggesting the occurrence of their cross-reactions. For the ACs, the C═O and C–N functional groups largely disappeared due to the intensive cracking reactions in the activation,[23] except the former in AC-B1-K3 and the latter functionality in AC-P1-K3. The vanishing of these functional groups could be due to the cross-polymerization reactions between PANI and the bio-oil.

The contact angle in Fig. S3† shows that the biochar was very hydrophobic. This was due to the limited pore development and the intense cracking for removing most polar functional groups. Although the AC activated from PANI (AC-P1-K3) showed the highest specific surface area, it was extremely hydrophobic, since there was a dearth of *o*-containing functionality. In contrast, the AC from the activation of the feedstock containing bio-oil was rather hydrophilic, which was related to the polar oxygen-containing functional groups derived from the bio-oil (Fig. 5b, FT-IR analysis). Apart from the polar functional groups, the high degree of pore development also contributed to the high hydrophilicity of the AC.

2.3.5 *In situ* DRIFTS analysis. *In situ* DRIFTS measurement of functional groups of the AC during the heating of the mixture of PANI and bio-oil in the presence or absence of $K_2C_2O_4$ is shown in Fig. 4a and b. The intensity variation of the typical absorption peaks is summarized in Fig. 4c to h. The –OH at 3535 cm^{-1} belonged to the phenolics from bio-oil, while the N–H at 3385 cm^{-1} and C–N at 1382 cm^{-1} were from PANI (Fig. 4a). The increasing temperature resulted in removal of –OH *via* cracking or dehydration reactions[33,34] and a similar tendency was observed for the N–H (Fig. 4c). Nonetheless, the decrease of the N–H absorption was relatively weak, which was attributed to its high thermal stability. Similarly, the retained high absorption abundance of olefinic ═C–H was also attributed to PANI. The abundance of C═O and its ratio to C═C decreased with the increase of heating temperature (Fig. S4a†), which was probably consumed *via* the cross-polymerization with PANI or cracking reactions.

The presence of $K_2C_2O_4$ significantly changed the abundance of functional groups by promoting the cracking reactions (Fig. 4b). Even at lower temperatures, the C–H in alkanes (2878 cm^{-1}) formed by cracking of aliphatic could be observed. In the meantime, the abundance of both N–H and –OH became much lower and further decreased through the cracking route with increasing temperature (Fig. 4f). $K_2C_2O_4$ also promoted cracking of carbonyl groups (1719 cm^{-1}), causing their large removal at 500 °C. Not all C═O were converted into the CO_2 (2309 cm^{-1}) intermediate, as some were transformed into CO (2055 cm^{-1}). In addition, the ratio of olefinic C═C located at 1610–1651 cm^{-1} to

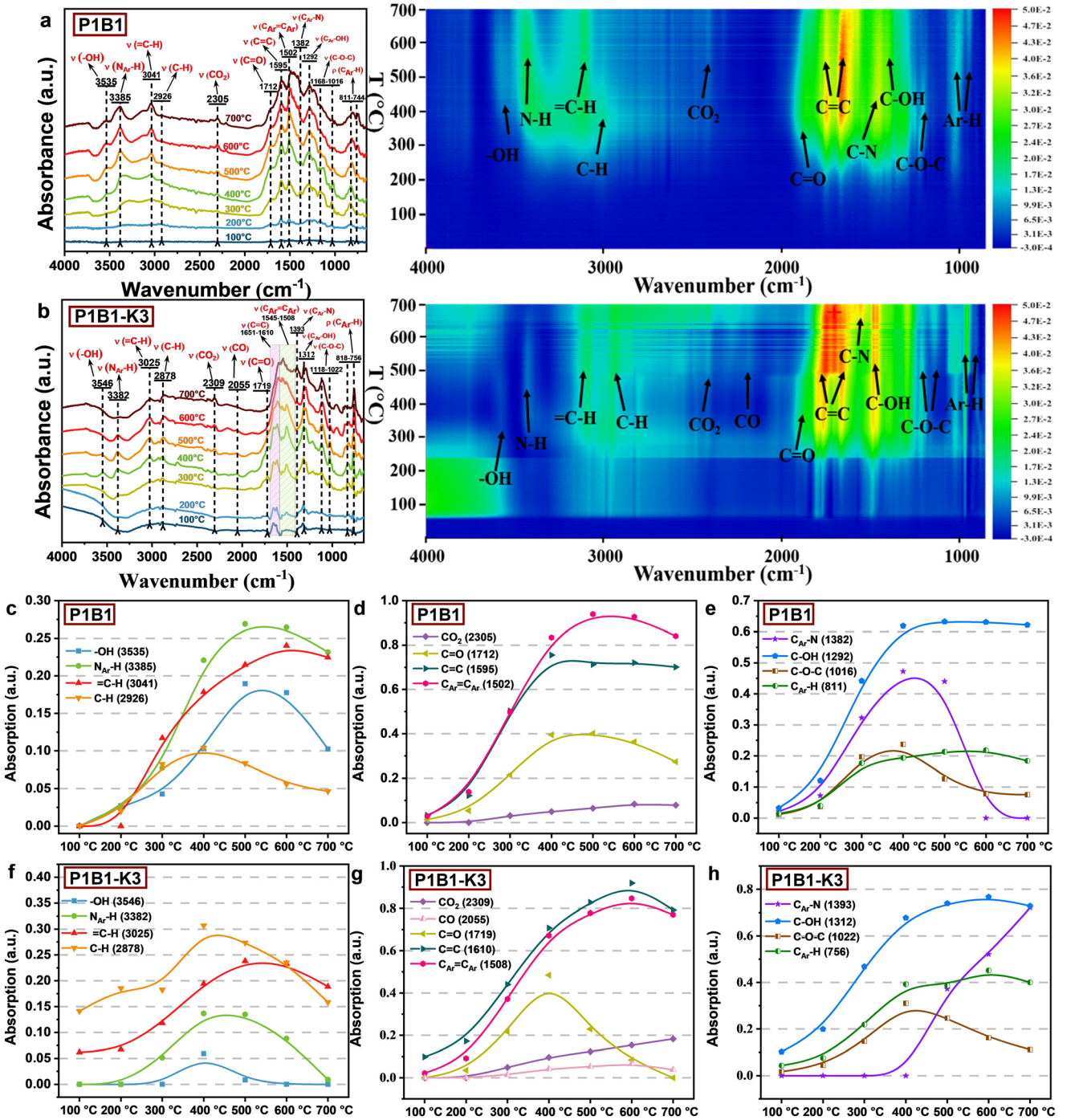

Fig. 4 *In situ* DRIFTS characterization for the functionalities of the biochar/AC in heating mixture of polyaniline and bio-oil in the (a and c–e) absence of $K_2C_2O_4$ and (b and f–h) presence of $K_2C_2O_4$.

aromatic C═C at 1502 cm^{-1} decreased with increasing temperature (Fig. S4b†). This indicated that the intensive cracking reactions induced by $K_2C_2O_4$ created some additional aliphatic structures. These excessive cracking reactions created the developed pore structures but also decreased the yield of the resulting AC.

2.3.6 SEM analysis. Fig. 5 and S5† show the microstructure of the feedstock, biochar and ACs characterized with SEM. The PANI feedstock was a cluster of numerous fine particles with a naturally rough surface (Fig. 5a1 and a2). The surface of bio-oil was smooth and flat, as it contained abundant heavy paste-like pyrolytic lignin (Fig. 5b1 and b2). For the biochar from the pyrolysis of PANI and bio-oil, the morphology showed similar paste-like materials of smooth surface but with layered structures (Fig. 5c1 and c2). Some heavy organics from the bio-oil clearly covered the potentially coarse surface

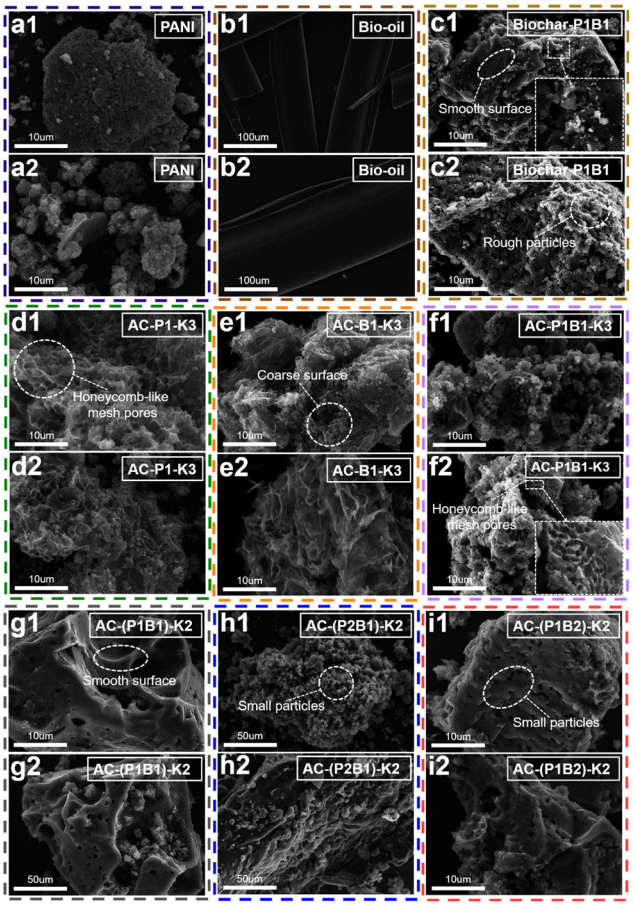

Fig. 5 SEM characterization of the feedstock, biochar and activated carbon produced from the activation of polyaniline, bio-oil or their mixture of different mass ratios at 800 °C; (a1 and a2) polyaniline; (b1 and b2) bio-oil; (c1 and c2) biochar-P1B1; (d1 and d2) AC-P1-K3; (e1 and e3) AC-B1-K3; (f1 and f2) AC-P1B1-K3; (g1 and g2) AC-(P1B1)-K2; (h1 and h2) AC-(P2B1)-K2; (i1 and i2) AC-(P1B2)-K2.

derived from the pyrolysis of PANI. After activation of PANI with $K_2C_2O_4$, the surface of AC exhibited honeycomb-like mesh pores (Fig. 5d1 and d2), which were formed by the etching effects of the potassium salts.[35,36] Although the morphology of the bio-oil was paste-like, the derived AC demonstrated a very coarse surface (Fig. 5e1 and e2) due to the intensive cracking/gasification reactions. For the AC-P1B1-K3 from direct activation of the mixture of PANI and bio-oil with $K_2C_2O_4$, the surface also became very fragmented and some hierarchical pore structures were observed (Fig. 5f1 and f2). Although cross-polymerization between PANI and the organics in the bio-oil occurred, their activation could still proceed smoothly, forming even more pores (Table 1, entry 4). Nonetheless, with the pre-polymerization, the activation of PANI and bio-oil with the mass ratio of 1 : 1 or 1 : 2 formed AC-(P1B1)-K2 and AC-(P1B2)-K2 with a smooth surface (Fig. 5g1, g2, i1 and i2), which was paste-like material and similar to that of the biochar (Fig. 5a1 and a2). The pre-polymerization formed the organics with high resistivity towards cracking, which explained their lower specific surface area. In comparison, even after the pre-polymerization, the activation of PANI and bio-oil with a mass ratio of 2 : 1 formed AC-(P2B1)-K2 with a broken surface decorated with lots of small particles (Fig. 5h1 and h2). Higher concentration of PANI did not facilitate the cross-polymerization, forming AC-(P2B1)-K2 with higher specific surface area but lower mass yield.

2.4 Application of AC

2.4.1 Phenol adsorption. Fig. 3h shows the adsorption performance of the biochar and the ACs towards phenol in aqueous solution. The biochar obtained from the pyrolysis of PANI and bio-oil exhibited very poor capability for adsorption of phenol, which was related to its limited pore structures (79.1 $m^2\ g^{-1}$). The activation of the single or mixed feedstock with $K_2C_2O_4$ promoted the development of pores, improving the adsorption capacity of AC. The increase of loading of AC provided more adsorption sites, promoting the adsorption of phenol. Although AC-P1-K3 possessed the highest specific surface area (2060.6 $m^2\ g^{-1}$), it showed inferior capability for the adsorption of phenol. The pore structure was not a determining factor for phenol adsorption, and the lower efficiency of AC-P1-K3 for adsorption of phenol from aqueous solution was related to its high hydrophobicity. In comparison, AC-P1B1-K3 with high abundance of micropores and also high hydrophilicity showed superior performance for adsorption. Additionally, AC-B1-K3 from activation of bio-oil also showed high capability for adsorption of phenol, although the specific surface area was only 1295.1 $m^2\ g^{-1}$. The abundance of oxygen-containing functional groups on the surface of AC resulted from the bio-oil (Fig. 5b) that provided the adsorption sites for phenol adsorption. The adsorption capacity of phenol for the ACs obtained with the pre-polymerization was roughly related to its specific surface area.

2.4.2 Hydrogenation of *o*-chloronitrobenzene/vanillin. Tables S2 and S3† show the catalytic performance of AC or biochar as a carrier of nickel catalyst for the hydrogenation of *o*-chloronitrobenzene and vanillin. During the hydrogenation of *o*-chloronitrobenzene, the conversion approached 100% over all the catalysts, generating the main product *o*-chloroaniline and also the by-product aniline (Table S3†). PANI contained a large amount of N element (Fig. 4), which might form complexation bonds with Cl during the hydrogenation process,[37] improving the catalytic activity of the catalysts, including the Ni/biochar with the biochar carrier of limited specific surface area. More aniline by-product was generated in the hydrogenation reaction catalyzed by the Ni/AC catalysts. AC had developed pore structures, which facilitated the dispersion of nickel and promoted dichlorination *via* hydrogenation. The hydrogenation of vanillin at 170 °C over the Ni/AC catalysts produced mainly 2-methoxy-4-methylphenol (MMP) (Table S4†). The catalysts were active and the conversion of vanillin reached 100%. The well-developed pore structures of AC provided sufficient anchoring sites for dispersion of Ni, rendering the high catalytic activity. In

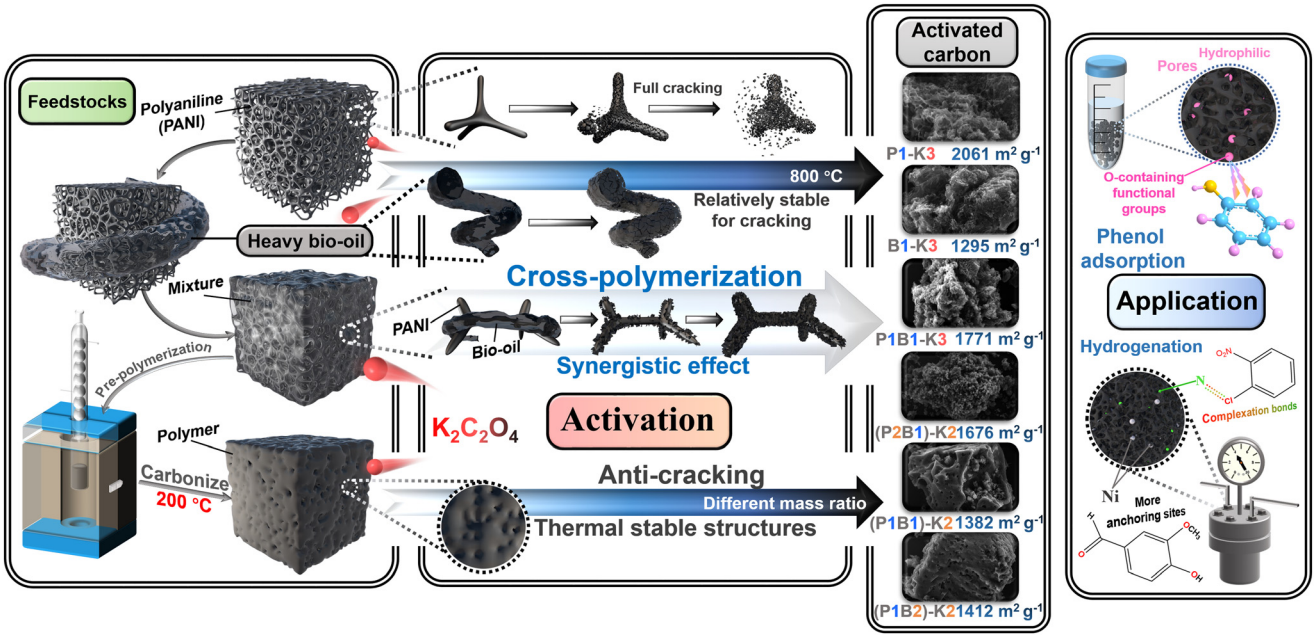

Scheme 2 Proposed different interactions between PANI and bio-oil during activation as well as the mechanisms for phenol adsorption and catalysis of hydrogenation.

contrast, the Ni/biochar catalyst with the biochar carrier of limited pore structures showed low activity for hydrogenation of vanillin.

3 Limitations and prospect

The aforementioned findings demonstrated that cross-interactions occurred in pre-polymerization at 200 °C or activation of the mixture of PANI and bio-oil with $K_2C_2O_4$ at 800 °C. This enhanced the yields of AC but did not remarkably increase or even reduce pore development during the activation, especially for the samples *via* the pre-polymerization pretreatment. However, the presence of bio-oil did enhance the hydrophilicity and hence performance for adsorption. This indicated that there were good sustainable application prospects of AC derived from PANI doped with bio-oil. Nonetheless, some remaining questions are to be further answered. Firstly, how the organics in the bio-oil react with PANI during direct heating of the mixture or the pre-polymerization needs to be clarified, as this impacts pore development and retainment of organics in the subsequent activation. Secondly, the cross-interaction of bio-oil and PANI is confirmed herein, influence of which on the properties of AC is also demonstrated from the above results. The unresolved issue herein is how these organics formed from the cross-polymerization reactions between PANI and bio-oil affect the pore development. The reason underneath the higher resistivity towards cracking reactions during the activation needs to be further explored. Thirdly, bio-oil is oxygen-rich while PANI is nitrogen-rich. How the oxygen- and nitrogen-containing species evolve in the activation needs to be further verified. This affects the distribution of functionalities on the surface of AC and also further application of AC as an adsorbent or carrier of catalyst.

4 Conclusions

In summary, activation of PANI, bio-oil or their mixture with or without pre-polymerization with $K_2C_2O_4$ as an activating agent was studied, aiming to probe the potential influence of cross-reactions of the two feedstocks of varied origin on the evolution of pore structures of AC as shown in Scheme 2. The results showed that direct activation of the mixture of PANI and bio-oil enhanced the yield of AC by 15% (with calculated average as a base) due to cross-polymerization occurring between PANI and organics in the bio-oil. Such cross-polymerization also showed synergistic effects in enhancing the specific surface area of the resultant AC from 1677.9 $m^2\ g^{-1}$ (calculated average) to 1771.3 $m^2\ g^{-1}$, also with more micropores generated. Nevertheless, the pre-polymerization pretreatment of PANI and bio-oil at 200 °C generated thermally more stable organics, enhancing their resistivity towards cracking/gasification in the activation. This enhanced the yield of AC from heating directly the mixture of PANI and bio-oil from 15.0% to 23.3% *via* the pre-polymerization plus activation, which, however, diminished the pore development and also generated more micropores. The pre-polymerization formed the carbon crystal structure in the resulting AC with less lattice distortion and retained more oxygen species. This made AC of highly hydrophilic nature, rendering superior capability for adsorption of phenol to that of the hydrophobic AC derived from activation of PANI, despite the higher specific surface area (AC–PANI, 2060.6 $m^2\ g^{-1}$). Additionally, the activation of PANI with $K_2C_2O_4$ formed AC with a coarse

surface such as honeycomb-like structures. The mixing of PANI with bio-oil and the pre-polymerization pretreatment formed AC of smooth surface due to coverage of the surface of AC with heavy components of bio-oil. This enhanced the yield of AC at the expense of pore development but increased the hydrophilicity for adsorption of polar organics. In addition, the developed pore structures of AC provided abundant anchoring points for Ni, which effectively catalyzed the hydrogenation of *o*-chloronitrobenzene and vanillin (conversion rate reached 100%). The results herein demonstrated the cross-interactions of bio-oil with PANI during activation, but the detailed reaction network needs to be further investigated.

5 Materials and methods

5.1 Materials

PANI and $K_2C_2O_4$ were purchased from Shanghai Macklin Biochemical Co., Ltd, while ethanol was bought from Sinopharm Chemical Reagent Co., Ltd. Heavy bio-oil was produced by the pyrolysis of wheat straw at 500 °C, the detailed composition of which can be found in a previously published paper.[38]

5.2 Experimental process

5.2.1 Pre-polymerization and activation experiments. For the pre-polymerization treatment, PANI was mixed with bio-oil in a mass ratio of 1 : 1, 1 : 2 and 2 : 1, which was then heated at 200 °C for 4 h in a tube furnace with a condensing unit at a heating rate of 20 °C min^{-1}, as shown in Fig. S1.† The pretreated samples were then dried in a 90 °C oven and then impregnated with $K_2C_2O_4$ with a mass ratio of 1 : 2. In addition, four control experiments, in which polyaniline and heavy bio-oil were directly impregnated with $K_2C_2O_4$ in different mass ratios without pre-polymerization, were also conducted for comparison. Before the subsequent activation experiment, all the prepared samples were dried to a constant weight in an oven at 90 °C and ground to the same particle size (30–100 μm).

Both pyrolysis and activation experiments were conducted in a fixed bed reactor equipped with a quartz tube of 20 mm diameter under a N_2 atmosphere (60 mL min^{-1}). Typically, 5 g of mixture were placed in a quartz sleeve with a diameter of 18 mm, which was then fixed in the central heating area of the quartz reactor. Before the start of the activation, the carrier gas was introduced about 15 min in advance to flush the residual air inside the tube. The sample was then heated to 800 °C at 5 °C min^{-1} and held at 800 °C for 1 h. The condensable volatiles (bio-oil) generated during the activation were captured by two empty gas–liquid separators connected to the end of the quartz reactor, and the non-condensable volatiles were further trapped by a third gas–liquid separator filled with ethanol. A 15 L gas bag was additionally connected to the outlet of the third gas–liquid separator to collect gaseous products. After completion of the experiment and cooling of the reactor, the solid products were collected from the quartz sleeve and then washed and stirred with 1 mol L^{-1} hydrochloric acid for 12 h to remove retained inorganics to obtain AC. The calculation method for the yield of the products is shown by eqn (1)–(3). To guarantee that the experimental error was less than 5%, every experiment was conducted more than three times.

$$Y_{\text{AC or Biochar}} = m_{\text{AC or Biochar}} \times 100/m_{\text{mixture}} \quad (1)$$

where $m_{\text{AC or Biochar}}$ is the mass of activated carbon or biochar after activation or pyrolysis; m_{mixture} is the mass of PANI and bio-oil mixed with different mass ratios after pre-polymerization (if any) or drying.

$$Y_{\text{bio-oil}} = m_{\text{bio-oil}} \times 100/m_{\text{mixture}} \quad (2)$$

where $m_{\text{bio-oil}}$ is the mass of bio-oil after reaction; m_{mixture} is the mass of PANI and bio-oil mixed with different mass ratios after pre-polymerization (if any) or drying.

$$Y_{\text{gas}} = 100\% - Y_{\text{AC or Biochar}} - Y_{\text{bio-oil}} \quad (3)$$

5.3 Characterization

5.3.1 Characterization of gas and bio-oil. The gaseous products were measured using a GC-7920 instrument (Zhongjiao Jinyuan, China). The light organics in the bio-oil were detected by a GC-MS instrument (Shimadzu, QP2020) with a capillary column of 30 m in length and an inner diameter of 0.25 mm, and identified by the standard NIST 2014 library. Their relative abundance was normalized by comparison to the peak area of the internal standard (methyl myristate). A UV fluorescence spectrometer (Shimadzu, rf-6000, Japan) was used to analyze the heavier organics with large π-conjugated structures in bio-oil.

5.3.2 Characterization of biochar and activated carbon. The BET method was used to calculate the pore characteristic parameters of biochar/AC obtained from the nitrogen adsorption–desorption measurement (Biaode SSA-6000, China). The crystal structure and microstructure of biochar/AC were analyzed by XRD (Ultima IV-2036E102, Japan) and SEM (EM-30, South Korea), respectively. The composition and distribution of elements in AC were analyzed using a EuroEA3000 – Single instrument. A contact angle goniometer (Powereach JC2000D1, China) was used to test the surface hydrophilicity of biochar/ACs. The abundance and the *in situ* change trend of functional groups on the surface of the biochar/AC during pyrolysis/activation were detected using Fourier-transform infrared (FT-IR) spectroscopy (NicoletiS50, USA).

5.4 Adsorption experiment

The adsorption capacity of AC for phenol was determined in an aqueous solution. The prepared phenol solution (30 mL and 50 mg L^{-1}) was mixed with AC of different loadings in a centrifuge tube, which was then placed in a shaker to vibrate

at a constant rate of 200 r min^{-1} for 1 h. The shaken centrifuge tubes were fixed in a centrifuge and separated at 10 000 RPM for 5 min, and then the supernatant was extracted using a 0.22 μm membrane filter. The phenol concentration in the solution after adsorption was calculated by the variation of peak intensity at 270 nm measured by an ultraviolet-visible spectrometer (AA-7000 Shimadzu, Japan). Eqn (4) and (5) display the adsorption ability (q_e, mg g^{-1}) and the removal efficiency (R, %) of the contaminants.

$$q_e = (C_o - C_e)V/m \quad (4)$$

$$R = (C_o - C_e)/C_o \times 100 \quad (5)$$

where C_o is the phenol concentration before adsorption; C_e is the phenol concentration that remains after adsorption; V is the volume placed into the adsorption tube; m is the amount of various adsorbents.

5.5 Hydrogenation experiment

The AC/biochar samples obtained from activation/pyrolysis of different feedstocks were used as a carrier of nickel catalyst by impregnating a certain mass of $Ni(NO_3)_2{\cdot}6H_2O$ to achieve a Ni loading of 15%. The impregnated sample was then dried in an oven at 90 °C for obtaining the precursor of the catalyst, which was placed in a tube furnace, heated to 500 °C in a N_2 atmosphere at a heating rate of 5 °C min^{-1}, and held at the end for 2 h. Finally, the calcined catalyst was reduced at 500 °C in a H_2 atmosphere (60 mL min^{-1}) for 2 h to obtain the Ni/AC catalyst. The hydrogenation experiment with Ni/AC as a catalyst was carried out in an autoclave reactor with a volume of 10 mL. The 4 g substrate–solvent mixture with a concentration of the target reactant (vanillin or *o*-chloronitrobenzene) of 2.5 wt% was added into the reactor with loading of catalyst of 40 mg. Before heating, the autoclave reactor was flushed with H_2 three times to remove residual air and then pressurized to 4 MPa with H_2. The hydrogenation experiment was carried out for 2 h at 170 °C. The liquid product was collected and analyzed by GC-MS (Shimadzu, QP2020) to calculate the conversion or yields of products.

Abbreviation

AC	Activated carbon
PANI	Polyaniline
P1B1	Polyaniline and bio-oil mixed at a mass ratio of 1 : 1
P1-K3	Polyaniline and $K_2C_2O_4$ mixed at a mass ratio of 1 : 3
B1-K3	Bio-oil and $K_2C_2O_4$ mixed at a mass ratio of 1 : 3
P1B1-K3	Polyaniline, bio-oil and $K_2C_2O_4$ mixed at a mass ratio of 1 : 1 : 3
(P1B1)-K2	Polyaniline and bio-oil pre-polymerized at a ratio of 1 : 1 and then mixed with $K_2C_2O_4$ at a ratio of 1 : 2
(P2B1)-K2	Polyaniline and bio-oil pre-polymerized at a ratio of 2 : 1 and then mixed with $K_2C_2O_4$ at a ratio of 1 : 2
(P1B2)-K2	Polyaniline and bio-oil pre-polymerized at a ratio of 1 : 2 and then mixed with $K_2C_2O_4$ at a ratio of 1 : 2
GC-MS	Gas chromatography-mass spectrometry
UV	UV-fluorescence spectroscopy
BET	Brunnauer–Emmet–Teller
XRD	X-ray diffraction
FT-IR	Fourier-transform infrared
DRIFTS	Diffuse reflectance infrared Fourier-transform spectroscopy
HHV	Higher heating value
SEM	Scanning electron microscopy
MMP	2-Methoxy-4-methylphenol
EMP	4-(Ethoxymethyl)-2-methylphenol

Author contributions

Baihong Li: conceptualization; investigation; formal analysis; conducted the experiments and data/evidence collection; writing – original draft; writing – review & editing. Chao Li: formal analysis, verified the accuracy of the results. Dianqiang Li: formal analysis; validation. Lijun Zhang: formal analysis; investigation. Shu Zhang: supervision; project administration. Yi Wang: supervision; modified the manuscript. Song Hu: supervision; modified the manuscript. Jun Xiang: supervision; modified the manuscript. Mortaza Gholizadeh: project administration; modified the manuscript. Xun Hu: resources; supervision; writing – review & editing; guided experimental plans; funding acquisition.

Conflicts of interest

The authors declare that they have no known competing financial interests or personal relationships that could have appeared to influence the work reported in this paper.

Acknowledgements

This work was supported by the National Natural Science Foundation of China (No. 52276195), the Program for supporting innovative research from Jinan (202228072), and the Program of agricultural development from Shandong (SD2019NJ015).

References

1 C. J. Wrasman, A. N. Wilson, O. D. Mante, K. Iisa, A. Dutta, M. S. Talmadge, D. C. Dayton, S. Uppili, M. J. Watson, X. Xu, M. B. Griffin, C. Mukarakate, J. A. Schaidle and M. R. Nimlos, Catalytic pyrolysis as a platform technology for supporting the circular carbon economy, *Nat. Catal.*, 2023, **6**, 563–573.

2 W. Cai, X. Wang, Z. Zhu, R. Kumar, P. N. Amaniampong, J. Zhao and Z.-T. Hu, Synergetic effects in the co-pyrolysis of

lignocellulosic biomass and plastic waste for renewable fuels and chemicals, *Fuel*, 2023, **353**, 129210.
3 J. He, Q. Qiang, L. Bai, W. Su, H. Yu, S. Liu and C. Li, Acetalization strategy in biomass valorization: a review, *Ind. Chem. Mater.*, 2024, **2**, 30–56.
4 W. Chaiwat, R. Gunawan, M. Gholizadeh, X. Li, C. Lievens, X. Hu, Y. Wang, D. Mourant, A. Rossiter, J. Bromly and C.-Z. Li, Upgrading of bio-oil into advanced biofuels and chemicals. Part II. Importance of holdup of heavy species during the hydrotreatment of bio-oil in a continuous packed-bed catalytic reactor, *Fuel*, 2013, **112**, 302–310.
5 H. Shahbeik, A. Shafizadeh, V. K. Gupta, S. S. Lam, H. Rastegari, W. Peng, J. Pan, M. Tabatabaei and M. Aghbashlo, Using nanocatalysts to upgrade pyrolysis bio-oil: A critical review, *J. Cleaner Prod.*, 2023, **413**, 137473.
6 S. Singh, K. K. Pant and M. Krishania, Current perspective for bio-oil production from agricultural residues in commercialization aspect: A review, *J. Anal. Appl. Pyrolysis*, 2023, **175**, 106160.
7 X. Hu and G. Lu, Bio-oil steam reforming, partial oxidation or oxidative steam reforming coupled with bio-oil dry reforming to eliminate CO2 emission, *Int. J. Hydrogen Energy*, 2010, **35**, 7169–7176.
8 P. Lahijani, M. Mohammadi, A. R. Mohamed, F. Ismail, K. T. Lee and G. Amini, Upgrading biomass-derived pyrolysis bio-oil to bio-jet fuel through catalytic cracking and hydrodeoxygenation: A review of recent progress, *Energy Convers. Manage.*, 2022, **268**, 115956.
9 M. Gholizadeh, S. Zhang, X. Hu and Y. Wang, Advances and Perspectives of Bio-oil Hydrotreatment for Biofuel Production, *Energy Fuels*, 2023, **37**, 10134–10154.
10 Y. Han, B. A. Simmons and S. Singh, Perspective on oligomeric products from lignin depolymerization: their generation, identification, and further valorization, *Ind. Chem. Mater.*, 2023, **1**, 207–223.
11 H. Fan, S. Zhou, Q. Li, G. Gao, Y. Wang, F. He, G. Hu and X. Hu, Hydrogen-bonded frameworks crystals-assisted synthesis of flower-like carbon materials with penetrable *meso*/macropores from heavy fraction of bio-oil for Zn-ion hybrid supercapacitors, *J. Colloid Interface Sci.*, 2021, **600**, 681–690.
12 Y. Chhiti, S. Salvador, J.-M. Commandre and F. Broust, Thermal decomposition of bio-oil: Focus on the products yields under different pyrolysis conditions, *Fuel*, 2012, **102**, 274–281.
13 Z. Xiong, Y. Wang, S. S. A. Syed-Hassan, X. Hu, H. Han, S. Su, K. Xu, L. Jiang, J. Guo, E. E. S. Berthold, S. Hu and J. Xiang, Effects of heating rate on the evolution of bio-oil during its pyrolysis, *Energy Convers. Manage.*, 2018, **163**, 420–427.
14 X. Li, H. Zhang, B. Zhao and Y. Zhang, Preparation of hydrogen storage carbon materials using bio-oil heavy components as carbon-containing precursor, *Fuel Process. Technol.*, 2020, **203**, 106386.
15 X. Hu, K. Nango, L. Bao, T. Li, M. D. M. Hasan and C.-Z. Li, High yields of solid carbonaceous materials from biomass, *Green Chem.*, 2019, **21**, 1128–1140.
16 X. Chen, H. Yang, Y. Chen, W. Chen, T. Lei, W. Zhang and H. Chen, Catalytic fast pyrolysis of biomass to produce furfural using heterogeneous catalysts, *J. Anal. Appl. Pyrolysis*, 2017, **127**, 292–298.
17 B. Hu, A.-s. Cheng, W.-l. Xie, J. Liu, Y.-b. Huang, L.-j. Zhu, B. Zhang, M.-x. Li, L. Zhao, T.-p. Wang and Q. Lu, The oxalic acid-assisted fast pyrolysis of biomass for the sustainable production of furfural, *Fuel*, 2022, **322**, 124279.
18 K. J. Yong, T. Y. Wu, C. B. T. L. Lee, Z. J. Lee, Q. Liu, J. M. Jahim, Q. Zhou and L. Zhang, Furfural production from biomass residues: Current technologies, challenges and future prospects, *Biomass Bioenergy*, 2022, **161**, 106458.
19 P. Delliere and N. Guigo, Revealed pathways of furan ring opening and surface crosslinking in biobased polyfurfuryl alcohol, *Eur. Polym. J.*, 2023, **187**, 111869.
20 X. Zhang, Y. Shao, K. Sun, M. Fan, S. Zhang and X. Hu, Introduction of NiSO4 to Ni/SiO2 catalyst in hydrogenation of furfuryl alcohol: Tailoring metallic nickel sites to switch major product from tetrahydrofurfuryl alcohol to cyclopentanone, *Mol. Catal.*, 2023, **542**, 113136.
21 E. Andini, J. Bragger, S. Sadula and D. G. G. Vlachos, Production of neo acids from biomass-derived monomers, *Green Chem.*, 2023, **25**, 3493–3502.
22 W. Chen and H.-Q. Yu, Advances in the characterization and monitoring of natural organic matter using spectroscopic approaches, *Water Res.*, 2021, **190**, 116759.
23 B. Li, C. Li, D. Li, L. Zhang, S. Zhang, Z. Cui, D. Wang, Y. Tang and X. Hu, Activation of pine needles with zinc chloride: Evolution of functionalities and structures of activated carbon versus increasing temperature, *Fuel Process. Technol.*, 2023, **252**, 107987.
24 J. Liang, C. Li, K. Sun, S. Zhang, S. Wang, J. Xiang, S. Hu, Y. Wang and X. Hu, Activation of mixed sawdust and spirulina with or without a pre-carbonization step: Probing roles of volatile-char interaction on evolution of pyrolytic products, *Fuel Process. Technol.*, 2023, **250**, 107987.
25 Q. Yao, Q. Wang, L. Wang, Y. Wang, J. Sun, H. Zeng, Z. Jin, X. Huang and L. Chen, The synergic regulation of conductivity and Seebeck coefficient in pure polyaniline by chemically changing the ordered degree of molecular chains, *J. Mater. Chem. A*, 2014, **2**, 2634–2640.
26 M. Gusain, R. Nagarajan and S. K. Singh, Highly ordered polyaniline: synthesis, characterization and electrochemical properties, *Polym. Bull.*, 2020, **77**, 3277–3286.
27 J. Hou, X. Tu, X. Wu, M. Shen, X. Wang, C. Wang, C. Cao, H. Peng and G. Wang, Remarkable cycling durability of lithium-sulfur batteries with interconnected mesoporous hollow carbon nanospheres as high sulfur content host, *Chem. Eng. J.*, 2020, **401**, 126141.
28 J. Liang, C. Li, S. Zhang, B. A. Mohamed, L. Wang, J. Xiang, S. Hu, Y. Wang and X. Hu, Activation of poplar and spirulina with H3PO4: Marked influence of biological structures of the biomasses on evolution structure of activated carbon, *Fuel Process. Technol.*, 2023, **252**, 107986.
29 L. Fang, W. Yang, J. Hou, K. Zheng, A. Hussain, Y. Zhang, Z. Hou and X. Wang, Tofukasu-derived biochar with

interconnected and hierarchical pores for high efficient removal of Cr (VI), *BioChar*, 2023, **5**(1), 69.

30 J. Song, Z. Meng, X. Wang, G. Zhang, C. Bi and J. Hou, One-step microwave method synthesis of Fe_3O_4 nanoribbon@carbon composite for Cr (VI) removal, *Sep. Purif. Technol.*, 2022, **298**, 121530.

31 M. Trchova and J. Stejskal, Polyaniline: The infrared spectroscopy of conducting polymer nanotubes (IUPAC Technical Report), *Pure Appl. Chem.*, 2011, **83**, 1803–1817.

32 J. Hou, T. Jiang, X. Wang, G. Zhang, J.-J. Zou and C. Cao, Variable dimensional structure and interface design of g-C_3N_4/BiOI composites with oxygen vacancy for improving visible-light photocatalytic properties, *J. Cleaner Prod.*, 2021, **287**, 125072.

33 C. Li, Y. Li, Y. Shao, L. Zhang, S. Zhang, S. Wang, B. Li, Z. Cui, Y. Tang and X. Hu, Activation of biomass with volatilized KOH, *Green Chem.*, 2023, **25**, 2825–2839.

34 C. Li, J.-i. Hayashi, Y. Sun, L. Zhang, S. Zhang, S. Wang and X. Hu, Impact of heating rates on the evolution of function groups of the biochar from lignin pyrolysis, *J. Anal. Appl. Pyrolysis*, 2021, **155**, 105031.

35 M. Xia, W. Chen, J. Wu, Y. Chen, H. Yang, X. Chen, D. Zhu and H. Chen, Organic salt-assisted pyrolysis for preparation of porous carbon from cellulose, hemicellulose and lignin: New insight from structure evolution, *Fuel*, 2021, **291**, 120185.

36 C. Wang, D. Wu, H. Wang, Z. Gao, F. Xu and K. Jiang, Biomass derived nitrogen-doped hierarchical porous carbon sheets for supercapacitors with high performance, *J. Colloid Interface Sci.*, 2018, **523**, 133–143.

37 J. E. Del Bene, I. Alkorta and J. Elguero, Do nitrogen bases form chlorine-shared and ion-pair halogen bonds?, *Chem. Phys. Lett.*, 2011, **508**, 6–9.

38 M. Fan, Y. Shao, K. Sun, Y. Jiang, S. Zhang, Y. Wang, S. Hu, J. Xiang and X. Hu, Bio-oil as a carbon source for synthesis of pin-like cobalt catalyst for hydrogenation of o-chloronitrobenzene, *Fuel Process. Technol.*, 2023, **248**, 107814.